JP Journal of Heat and Mass Transfer

https://pphmjopenaccess.com
https://doi.org/10.17654/0973576326011 **P-ISSN: 0973-5763**
Volume 39, Number 1, February 2026, Pages 197-214 **E-ISSN: 3049-2556**

HIEMENZ FLOW OF TETRA NANOFLUID ON A SHRINKING SURFACE

Najiyah Safwa Khashi'ie[1,*], Iskandar Waini[2], Abdul Rahman Mohd Kasim[3], Nur Syahirah Wahid[4], Norihan Md Arifin[4] and Didit Adytia[5]

[1]Fakulti Teknologi dan Kejuruteraan Mekanikal
Universiti Teknikal Malaysia Melaka
Hang Tuah Jaya, 76100 Durian Tunggal
Melaka, Malaysia
e-mail: najiyah@utem.edu.my

[2]Fakulti Teknologi dan Kejuruteraan Industri dan Pembuatan
Universiti Teknikal Malaysia Melaka
Hang Tuah Jaya, 76100 Durian Tunggal
Melaka, Malaysia

[3]Centre for Mathematical Sciences
Universiti Malaysia Pahang Al-Sultan Abdullah
Gambang, 26300 Kuantan
Pahang, Malaysia

Received: January 8, 2026; Accepted: February 12, 2026

Keywords and phrases: dual solutions, Hiemenz flow, heat transfer, tetra hybrid nanofluid, shrinking surface, stagnation point flow.

*Corresponding author

How to cite this article: Najiyah Safwa Khashi'ie, Iskandar Waini, Abdul Rahman Mohd Kasim, Nur Syahirah Wahid, Norihan Md Arifin and Didit Adytia, Hiemenz flow of tetra nanofluid on a shrinking surface, JP Journal of Heat and Mass Transfer 39(1) (2026), 197-214. https://doi.org/10.17654/0973576326011

Published Online: February 24, 2026

[4]Department of Mathematics and Statistics
Faculty of Science
Universiti Putra Malaysia
43400 UPM Serdang, Selangor, Malaysia

[5]School of Computing
Telkom University
Bandung, 40257, Indonesia

Abstract

This study examines the Hiemenz flow of a tetra hybrid nanofluid comprising aluminum oxide/alumina (Al_2O_3), copper (Cu), silicon dioxide/silica (SiO_2), and titanium dioxide/titania (TiO_2) nanoparticles suspended in a water-based fluid over a shrinking sheet, focusing on the effects of varying the velocity ratio parameter and nanoparticle volume fractions on key flow characteristics. The analysis evaluates skin friction, the Nusselt number (indicating heat transfer efficiency), velocity and temperature profiles. The governing equations are transformed into a system of ordinary differential equations (ODEs) via similarity transformations and solved numerically using the Matlab bvp4c solver. The results indicate that the skin friction is significantly influenced by changes in the velocity ratio parameter, while the tetra nanofluid demonstrates a superior thermal performance compared to ternary and binary nanofluids. Two distinct solutions are identified within specific parameter intervals. These findings underscore the advanced heat transfer capabilities and flow stability of the tetra nanofluid, particularly for combinations incorporating aluminum oxide, copper, silicon dioxide, and titanium dioxide nanoparticles.

1. Introduction

The effective thermal regulation in numerous engineering systems is crucial to ensure reliable performance and energy efficiency. Standard cooling medium in industry such as water, ethylene glycol and mineral oils is frequently utilized due to their chemical stability and ease of handling. Nonetheless, these fluids are inherently limited by their poor thermal

conductivity which restricts their application in demanding heat transfer operations. In response to this challenge, Choi and Eastman [1] introduced nanofluids which are formed by embedding nanoscale solid particles into a conventional base liquid (water/ethylene glycol/mineral oils) and yielding better thermal regulation properties in engineered systems. This innovation has led to an upsurge in research across various domains including both theoretical and experimental studies which enabled advanced applications such as heat exchangers, thermal control in microprocessors, solar energy systems and vehicle cooling circuits. With the growing demand for higher thermal performance, researchers advanced the concept further by introducing hybrid nanofluids composed of two dissimilar nanoparticles which offer combined advantages in terms of thermal and rheological enhancements. Subsequently, the emergence of ternary hybrid nanofluids, incorporating three types of nanoparticles has demonstrated even greater efficiency by leveraging multiphase synergy and optimized dispersion characteristics. The density analysis of ternary hybrid nanoparticles from Al_2O_3-ZnO-Fe_3O_4 was experimentally conducted by Adun et al. [2]. They recommended that future investigations should explore a broader range of nanoparticle mixing ratios in ternary nanofluids to better elucidate the influence of combining diverse nanoparticle types on thermal and flow characteristics. Meanwhile, Mohammed Zayan et al. [3] highlighted the thermal conductivity enhancement of GO-TiO_2-Ag/water and rGO-TiO_2-Ag/water ternary hybrid nanofluids up to 83% at low concentrations.

In line with this evolution, tetra nanofluids are then proposed which comprised of four distinct nanoparticles suspended in a base fluid. These complex nanoparticle blends are tailored to utilize the combined benefits of distinct materials, paving the way for innovation in high-performance thermal systems. Very recent, Khashi'ie et al. [4] showed that the skin friction and heat transfer coefficients of tetra hybrid nanofluid (Al_2O_3-Cu-SiO_2-TiO_2) were lower than the ternary hybrid nanofluid (Al_2O_3-Cu-TiO_2) when the numerical computations were tested for opposing boundary layer flow case. In addition, Elsherbiny et al. [5] experimentally studied the tetra

hybrid nanofluid flow comprising of Al_2O_3, CuO, ZnO, and Ag nanoparticles with distilled water as the base fluid in microprocessor cooling systems equipped with microchannel heat sinks. Many experimental and numerical studies were briefly discussed and conducted to investigate the behavior of these nanofluids (see Yuan et al. [6], Oladapo et al. [7], Adnan et al. [8] and Jamrus et al. [9-13]). Concurrently, flow models such as Hiemenz flow, which describe stagnation point behavior over planar surfaces, become highly relevant due to their role in processes such as coating technologies and cooling plates. The foundational works on Hiemenz-type stagnation point flow involving stretching/shrinking surfaces were examined by Aly and Usafzai [14], Zainal et al. [15] and Waini et al. [16] for hybrid nanofluid, Jamrus et al. [11], Ruslan et al. [17], Sarfraz and Khan [18] and Sachhin et al. [19] for the ternary hybrid nanofluid cases.

Motivated by recent advancements in nanoparticle-enhanced heat transfer, the present study aims to investigate the Hiemenz stagnation point flow over a shrinking surface using a tetra hybrid nanofluid system, incorporating four distinct nanoparticles (alumina-copper-silica-titania) suspended in water. The governing boundary layer equations (PDEs) are reduced to a system of ordinary differential equations (ODEs-similarity equations) via similarity transformation and solved numerically using MATLAB's bvp4c solver. A key feature of this study is the exploration of dual solutions, which arise under specific flow conditions and are critical to understanding flow stability in shrinking surface scenarios. In addition to the numerical modelling, a comprehensive comparative analysis is conducted to assess the thermal and momentum transport performance among hybrid, ternary and tetra nanofluid configurations under the same flow conditions. The novelty of this work lies in its combined focus on both the dual solution behavior and the hierarchical evaluation of nanoparticle configurations which has not been addressed in previous literature. The findings of this study provide deeper insights into the effect of multi-component nanoparticle suspensions on boundary layer characteristics and offer valuable implications for optimizing thermal systems where precise control of stagnation flow and heat transfer is required.

2. Problem Formulation

A basic Hiemenz flow and thermal characteristics of tetra hybrid nanofluid (alumina-copper-titania/water) are numerically studied subjected to a stretching/shrinking sheet. The flow geometry is illustrated in Figure 1 where the Cartesian coordinates (x, y) are considered. Free stream surface velocity is in the variable form of $U_e(x) = ax$, while that of stretching/shrinking in a variable form of $U_w(x) = bx$, where a and b are constants. Other assumption is all the nanoparticles dispersed in the base fluid are presumed to maintain thermal equilibrium and a uniform spatial distribution throughout the flow domain.

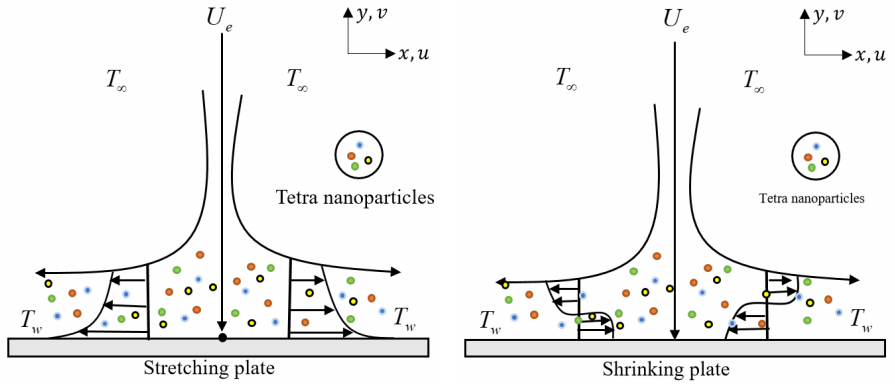

Figure 1. Physical model with coordinate system for (a) stretching case and (b) shrinking case.

The governing partial differential equations derived from the fundamental laws of momentum and energy conservation are adapted and extended from previously established nanofluid models to capture the distinctive thermofluidic behavior of the ternary hybrid system [16]:

$$\frac{\partial u}{\partial x} + \frac{\partial v}{\partial y} = 0, \tag{1}$$

$$u\frac{\partial u}{\partial x} + v\frac{\partial u}{\partial y} = U_e\frac{dU_e}{dx} + \frac{\mu_{ttnf}}{\rho_{ttnf}}\frac{\partial^2 u}{\partial y^2}, \tag{2}$$

$$u\frac{\partial T}{\partial x}+v\frac{\partial T}{\partial y}=\frac{k_{ttnf}}{(\rho C_p)_{ttnf}}\frac{\partial^2 T}{\partial y^2}, \tag{3}$$

$$u=U_w(x),\ v=0,\ T=T_w \text{ at } y=0$$

$$u\to U_e(x),\ T\to T_\infty \text{ as } y\to\infty. \tag{4}$$

In this numerical study, the velocity components are u and v for x- and y-coordinates, respectively, while T denotes the nanofluid's temperature:

$$\psi=(a\nu_f)^{1/2}xf(\eta),\quad \eta=y\left(\frac{a}{\nu_f}\right)^{1/2},\quad \theta(\eta)=\frac{T-T_\infty}{T_w-T_\infty}. \tag{5}$$

In equation (5), the stream function ψ and similarity variable η are used to derive the velocities such that

$$u=\partial\psi/\partial y=axf'(\eta),\quad v=-\partial\psi/\partial x=-(a\nu_f)^{1/2}f(\eta). \tag{6}$$

By applying the similarity transformations in equation (5), the boundary layer and energy equations (2)-(4) are transformed into a system of ordinary or similarity differential equations as outlined in Waini et al. [16] and Khashi'ie et al. [20]:

$$\frac{\mu_{ttnf}/\mu_f}{\rho_{ttnf}/\rho_f}f'''+ff''-f'^2+1=0, \tag{7}$$

$$\frac{1}{Pr}\frac{k_{ttnf}/k_f}{(\rho C_p)_{ttnf}/(\rho C_p)_f}\theta''+f\theta'=0, \tag{8}$$

$$f(0)=0,\quad f'(0)=\lambda,\quad \theta(0)=1,$$

$$f'(\eta)\to 1,\quad \theta(\eta)\to 0 \text{ as } \eta\to\infty, \tag{9}$$

where *Prandtl number* is defined as $Pr=\left(\frac{\mu C_p}{k}\right)_f$ and velocity ratio parameter $\lambda=\frac{b}{a}$, where $\lambda>0$ stands for the stretching plate (assisting flow), $\lambda<0$ denotes the shrinking plate (opposing flow) while $\lambda=0$ is for

a static plate. Table 1 compiles the effective properties of the tetra hybrid nanofluid formulated through empirical and theoretical considerations and widely used by many researchers (see Khan et al. [21] and Mahariq et al. [22]). For computational purposes, Table 2 details the thermophysical attributes of the base fluid and selected nanoparticles. These values are essential in initializing the numerical simulations of tetra hybrid nanofluid transport phenomena. In the table, the subscripts *ttnf*, *thnf*, *hnf*, *nf* and *f* represent tetra hybrid nanofluid, ternary hybrid nanofluid, hybrid nanofluid, single nanofluid and base fluid, respectively. Besides, *s*1, *s*2, *s*3 and *s*4 symbolize the first (alumina), second (copper), third (silica) and fourth (titania) nanoparticles, respectively, while ϕ_1, ϕ_2, ϕ_3 and ϕ_4 correspond to the volumetric concentration of first, second, third and fourth nanoparticles, respectively.

Table 1. Correlations of tetra hybrid nanofluid

Properties	Tetra hybrid nanofluid
Heat capacity	$(\rho C_p)_{ttnf} = (1-\phi_4)\left\{\begin{matrix}(1-\phi_3)\left[(1-\phi_2)\left(\begin{matrix}(1-\phi_1)(\rho C_p)_f \\ +\phi_1(\rho C_p)_{s1}\end{matrix}\right)+\phi_2(\rho C_p)_{s2}\right] \\ +\phi_3(\rho C_p)_{s3}\end{matrix}\right\}+\phi_4(\rho C_p)_{s4}$
Dynamic viscosity	$k_{ttnf} = k_{thnf}\left[\frac{k_{s4}+2k_{thnf}-2\phi_4(k_{thnf}-k_{s4})}{k_{s4}+2k_{thnf}+\phi_4(k_{thnf}-k_{s4})}\right]$, where $k_{thnf} = k_{hnf}\left[\frac{k_{s3}+2k_{hnf}-2\phi_3(k_{hnf}-k_{s3})}{k_{s3}+2k_{hnf}+\phi_3(k_{hnf}-k_{s3})}\right]$, $k_{hnf} = k_{nf}\left[\frac{k_{s2}+2k_{nf}-2\phi_2(k_{nf}-k_{s2})}{k_{s2}+2k_{nf}+\phi_2(k_{nf}-k_{s2})}\right]$, $k_{nf} = k_f\left[\frac{k_{s1}+2k_f-2\phi_1(k_f-k_{s1})}{k_{s1}+2k_f+\phi_1(k_f-k_{s1})}\right]$
Thermal conductivity	$\mu_{ttnf} = \frac{\mu_f}{\{(1-\phi_1)(1-\phi_2)(1-\phi_3)(1-\phi_4)\}^{2.5}}$
Density	$\rho_{ttnf} = (1-\phi_4)\{(1-\phi_3)[(1-\phi_2)((1-\phi_1)\rho_f+\phi_1\rho_{s1})+\phi_1\rho_{s2}]+\phi_3\rho_{s3}\}+\phi_4\rho_{s4}$

Table 2. Thermophysical properties of the base fluid and constituent nanoparticles

Thermophysical properties	H_2O	Al_2O_3	Cu	TiO_2	SiO_2
$\rho\,(\mathrm{kg/m^3})$	997.1	3970	8933	4250	2200
$k\,(\mathrm{W/mK})$	0.6130	40	400	8.9538	1.4013
$C_p\,(\mathrm{J/kgK})$	4179	765	385	686.2	754

The skin friction coefficient and local Nusselt number are given as

$$C_f = \frac{\left(\frac{\partial u}{\partial y}\right)_{y=0} \mu_{ttnf}}{\rho_f U_e^2}, \quad Nu_x = \frac{\left(-\frac{\partial T}{\partial y}\right)_{y=0} x k_{ttnf}}{k_f (T_w - T_\infty)}. \tag{10}$$

By incorporating the similarity transformations from equation (5) into the definitions provided in equation (10), the expressions for the skin friction coefficient and the Nusselt number are reformulated as follows:

$$Re_x^{-1/2} Nu_x = -\frac{k_{ttnf}}{k_f}\theta'(0),\ Re_x^{1/2} C_f = \frac{\mu_{ttnf}}{\mu_f} f''(0),\ Re_x = U_e(x)x/\nu_f. \tag{11}$$

3. Stability Analysis

Zainal et al. [23] and Aladdin et al. [24] provided an in-depth discussion on the flow stability past a moving plate case. By introducing a new similarity transformation that accounts for temporal variations, the governing equations specifically equations (2) and (3) are reformulated to include unsteady effects, leading to a more comprehensive mathematical model such that

$$\frac{\partial u}{\partial t} + u\frac{\partial u}{\partial x} + v\frac{\partial u}{\partial y} = U_e \frac{dU_e}{dx} + \frac{\mu_{ttnf}}{\rho_{ttnf}} \frac{\partial^2 u}{\partial y^2}, \tag{12}$$

$$\frac{\partial T}{\partial t} + u\frac{\partial T}{\partial x} + v\frac{\partial T}{\partial y} = \frac{k_{ttnf}}{(\rho C_p)_{ttnf}} \frac{\partial^2 T}{\partial y^2}, \tag{13}$$

while the suitable similarity transformation is

$$\psi = (a\nu_f)^{1/2} x f(\eta, \tau), \quad \eta = y\left(\frac{a}{\nu_f}\right)^{1/2}, \quad \theta(\eta, \tau) = \frac{T - T_\infty}{T_w - T_\infty}, \quad \tau = at. \tag{14}$$

Equations (12) and (13) as well as the boundary conditions are then simplified to

$$\frac{\mu_{ttnf}/\mu_f}{\rho_{ttnf}/\rho_f}\frac{\partial^3 f}{\partial \eta^3} + f\frac{\partial^2 f}{\partial \eta^2} - \left(\frac{\partial f}{\partial \eta}\right)^2 + 1 - \frac{\partial^2 f}{\partial \eta \partial \tau} = 0, \tag{15}$$

$$\frac{1}{Pr}\frac{k_{ttnf}/k_f}{(\rho C_p)_{ttnf}/(\rho C_p)_f}\frac{\partial^2 \theta}{\partial \eta^2} + f\frac{\partial \theta}{\partial \eta} - \frac{\partial \theta}{\partial \tau} = 0, \tag{16}$$

$$f(0, \tau) = 0, \quad \frac{\partial f(0, \tau)}{\partial \eta} = \lambda, \quad \theta(0, \tau) = 1,$$

$$\frac{\partial f(\eta, \tau)}{\partial \eta} \to 1, \quad \theta(\eta, \tau) \to 0 \text{ as } \eta \to \infty. \tag{17}$$

Then, following the methodology as outlined by Waini et al. [16], Zainal et al. [23] and Aladdin et al. [24], the disturbance/perturbation equations are introduced such that

$$f(\eta, \tau) = f_0(\eta) + e^{-\gamma\tau}F(\eta), \tag{18}$$

$$\theta(\eta, \tau) = \theta_0(\eta) + e^{-\gamma\tau}G(\eta). \tag{19}$$

Here, $f = f_0$, $\theta = \theta_0$, F and G are disturbance functions associated with f_0 and θ_0, respectively. The eigenvalue γ serves as an indicator of solution stability. The stability of the obtained solutions is governed by the smallest eigenvalue γ_1, where positive value of γ_1 signifies that the solution is physically realizable and stable over time. The resulting linearized eigenvalue problem, obtained after simplification, yields the governing equations and associated boundary conditions as follows:

$$\frac{\mu_{ttnf}/\mu_f}{\rho_{ttnf}/\rho_f}F''' + f_0F'' + Ff_0'' - 2f_0'F' + \gamma F' = 0, \tag{20}$$

$$\frac{1}{Pr}\frac{k_{ttnf}/k_f}{(\rho C_p)_{ttnf}/(\rho C_p)_f}G'' + F\theta_0' + f_0 G' + \gamma G = 0, \tag{21}$$

$$F(0) = F'(0) = G(0) = 0, \quad F'(\infty) \to 0, \quad G(\infty) \to 0. \tag{22}$$

To prevent the occurrence of zero eigenvalues using the linearized boundary condition (see equation (22)), Harris et al. [25] relaxed one of the boundary conditions as follows:

$$F(0) = F'(0) = G(0) = 0, \quad F''(0) = 1, \quad G(\infty) \to 0. \tag{23}$$

4. Results and Discussion

The solutions for the similarity equations (7)-(9) are numerically computed in determining the skin friction and heat transfer characteristics. The bvp4c function is being the main interface and embedded in the Matlab software in providing the similarity solutions from equations (7)-(9). The details of this solver in solving boundary value problems were highlighted by Khashi'ie et al. [4]. Dual solutions are generated for specific ranges of parameters as presented in Figures 2-4 which are the shrinking parameter $\lambda_c < \lambda \leq -1.2$ and volumetric concentration of alumina, copper, silica and titania nanoparticles, respectively, $\phi_1, \phi_2, \phi_3, \phi_4 = 0.01(1\%)$. In the validation process presented in Tables 3 and 4, the numerical results for the skin friction coefficient and the local Nusselt number/heat transfer coefficient are compared with published data from Waini et al. [16] and Ruslan et al. [17] to ensure the accuracy of the present model. For consistency and to enable a fair comparison, the following parameter values were held constant: Prandtl number $(Pr = 6.2)$ and volume fractions of silica and titania $(\phi_3 = \phi_4 = 0)$. Only the alumina (ϕ_1) and copper volume fractions (ϕ_2) were varied corresponding to the binary hybrid nanofluid scenario (Al_2O_3-Cu/water) as previously studied. The positive agreement between these results shows that the present model is precise and accurate. Although a grid independence test is not directly applicable due to the nature

of the bvp4c solver which uses an adaptive collocation method with built-in error control, the robustness of the numerical results is ensured by refining solver tolerance setting. The default relative error tolerance is RelTol = 1e-10. This convergence behavior ensures that the computed solutions are numerically stable and reliable. In addition, Tables 3 and 4 highlight only single solution available when $\lambda = -0, 5, 0, 0.5$ and it is also apparent that the addition of ϕ_1 and ϕ_2 enhances both skin friction and heat transfer coefficients. However, the results in Tables 3 and 4 are valid for the discussion of binary hybrid nanofluid (alumina-copper/water). Hence, this present study is essential to discuss the thermal and flow characteristics of tetra hybrid nanofluid with the inclusion of silica and titania nanoparticles.

Table 3. Data validation of $Re_x^{1/2}C_f$ given that $\phi_3 = \phi_4 = 0$

ϕ_2	λ	$Re_x^{1/2}C_f$ (Skin friction coefficient)					
		$\phi_1 = 0$			$\phi_1 = 0.05$		
		Present	Ruslan et al. [17]	Waini et al. [16]	Present	Ruslan et al. [17]	Waini et al. [16]
0	0	1.232588	1.232588	1.232588	1.408763	1.408763	1.408763
0.03	0	1.425110	1.425110	1.425110	1.605715	1.605715	1.605715
0.05	0	1.553850	1.553850	1.553850	1.738637	1.738637	1.738637
0.05	-0.5	1.885501	1.885501	1.885501	2.109729	2.109729	2.109729
0.05	0.5	0.899208	0.899208	0.899208	1.006144	1.006144	1.006144

Table 4. Data validation of $Re_x^{-1/2}Nu_x$ given that $\phi_3 = \phi_4 = 0$

ϕ_2	λ	$Re_x^{-1/2}Nu_x$ (Heat transfer coefficient)					
		$\phi_1 = 0$			$\phi_1 = 0.05$		
		Present	Ruslan et al. [17]	Waini et al. [16]	Present	Ruslan et al. [17]	Waini et al. [16]
0	0	1.127964	1.127964	1.127964	1.229275	1.229275	1.229275
0.03	0	1.213918	1.213918	1.213918	1.317395	1.317395	1.317395
0.05	0	1.269379	1.269379	1.269379	1.374810	1.374810	1.374810
0.05	-0.5	0.706314	0.706314	0.706314	0.791231	0.791231	0.791231
0.05	0.5	1.733859	1.733859	1.733859	1.856885	1.856885	1.856885

Figures 2 and 3 show the comparative analysis between alumina-copper/water binary hybrid nanofluid $(\phi_1, \phi_2 = 1\%, \phi_3 = \phi_4 = 0\%)$, alumina-copper-titania/water ternary hybrid nanofluid $(\phi_1, \phi_2, \phi_4 = 1\%, \phi_3 = 0\%)$ and alumina-copper-silica-titania/water tetra hybrid nanofluid with different concentrations $(\phi_3 = 0.5\%, 1\%)$. The role and significance of tetra hybrid nanofluid in enhancing the skin friction is clear in Figure 2 such that the value of $Re_x^{1/2} C_f$ increases as ϕ_3 increases. This trend can be attributed to the enhanced momentum diffusion due to the synergistic interaction among the four different nanoparticles which not only improves the thermal conductivity but also increases the effective viscosity of the nanofluid. This enhances the fluid's resistance to flow near the wall and thereby increasing the wall shear stress. The incorporation of silica which has a moderate thermal conductivity and relatively low density as compared to copper or alumina helps balance the fluid's inertia and thermal properties. The separation value λ_c or also called as *boundary layer separator* is same for all cases of hybrid nanofluid $(\lambda_c = -1.24657)$ which implies that all the nanofluids are influential in delaying the separation. Figure 2 also reveals that the tetra hybrid nanofluid has the greatest skin friction coefficient followed by ternary and binary hybrid nanofluids for each value of tested λ and this observation is seen for both first and second solutions. No significant difference is seen between ternary and tetra hybrid nanofluids in enhancing the heat transfer rate as illustrated in Figure 3. However, both ternary and tetra hybrid nanofluids have higher heat transfer than the binary hybrid nanofluid. The increment of ϕ_3 slightly reduces the heat transfer rate as $\lambda \to \lambda_c$ which implies that the ternary hybrid nanofluid has the maximum heat transfer. This can be explained by the thermal energy storage effect such that as more nanoparticles are introduced, the fluid gains a higher thermal capacity which allows it to retain more energy internally. Although the thermal conductivity increases, the temperature gradient at the wall may decrease due to this energy absorption and consequently, leading to a lower local Nusselt number. Surprisingly, different heat transfer characteristics are

observed when λ is far from the separation value λ_c. From Figures 2 and 3, it is also clear that as the value of λ increases and far from λ_c, both skin and heat transfer coefficients greatly increase.

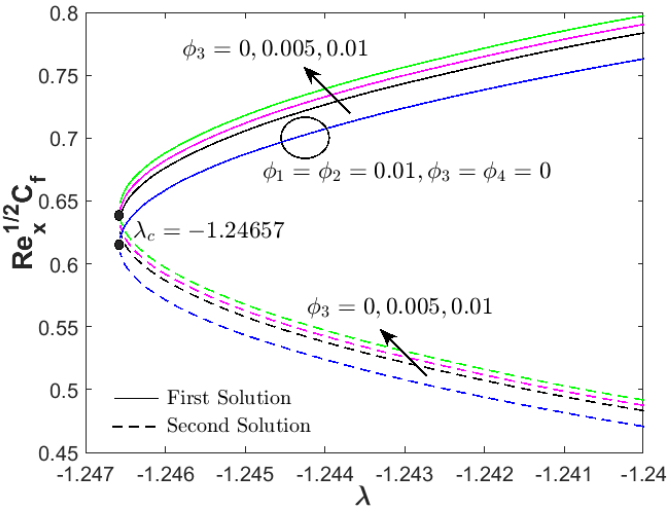

Figure 2. Skin friction towards λ with different ϕ_3.

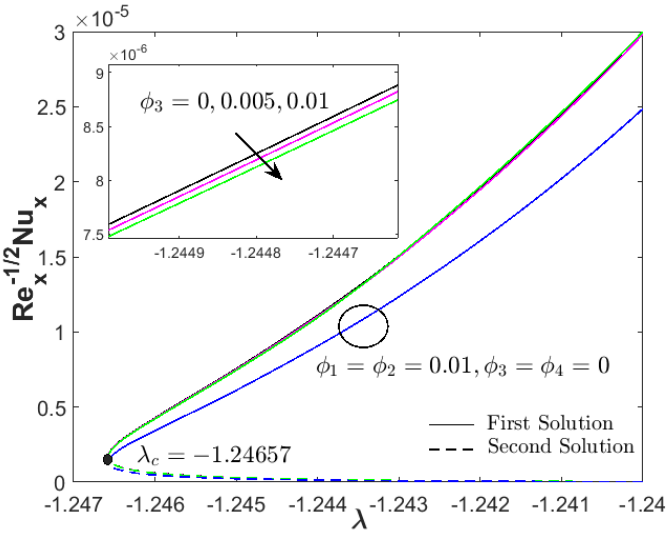

Figure 3. Heat transfer rate towards λ with different ϕ_3.

Figures 4 and 5 present the respective profiles of tetra hybrid nanofluid's velocity and temperature with different velocity ratio parameter. The profiles fulfill the far field boundary condition in equation (9) which also validates the reliability of present model. As $\lambda \to \lambda_c$, both velocity and temperature profiles decrease while the second solution shows opposite trend of profiles.

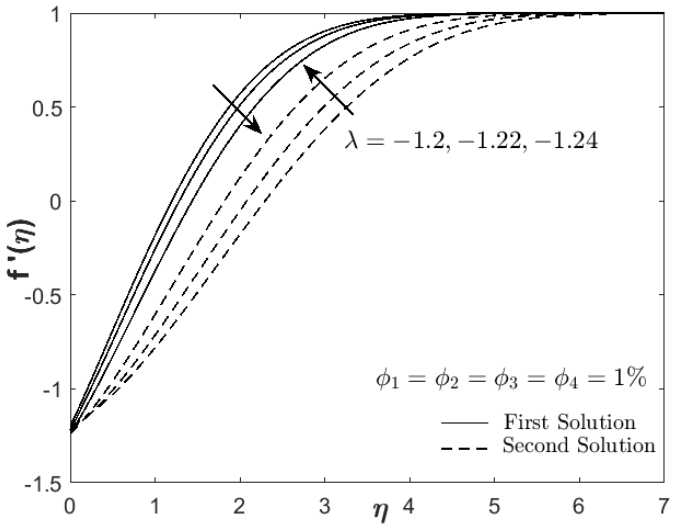

Figure 4. Velocity profile with different λ.

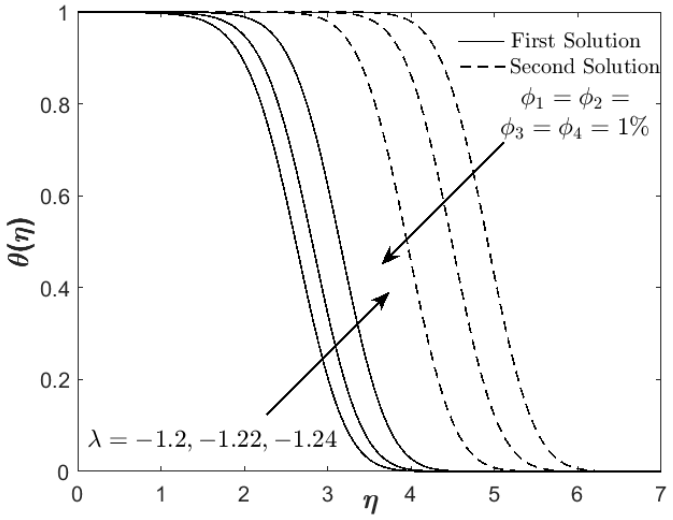

Figure 5. Temperature profile with different λ.

4. Conclusions

This study presents a numerical investigation of the Hiemenz stagnation point flow of tetra hybrid nanofluid over a shrinking surface, with emphasis on dual solution behavior and a comparative performance analysis against binary and ternary hybrid nanofluid models. The inclusion of four distinct nanoparticles which are alumina, copper, silica and titania within the base fluid demonstrates a clear enhancement in the skin friction coefficient particularly with the increasing of silica concentration. Although the heat transfer improvement of tetra nanofluid is only marginal as compared to the ternary system, both outperform the binary configuration. Dual solutions were observed under certain conditions with the first (stable) solution satisfying the far-field boundary criterion. The study confirms that tetra hybrid nanofluids can significantly improve flow resistance characteristics making them highly suitable for applications involving shrinking geometries. These findings contribute to a deeper understanding of multiphase nanofluid behavior and offer valuable insights for the design of next generation heat transfer systems.

Acknowledgements

We acknowledge research support from Universiti Teknikal Malaysia Melaka, Malaysia through international research matching grant: ANTARABANGSA(IRMG)-TEL-U/2025/FTKM/A00086.

References

[1] S. U. S. Choi and J. A. Eastman, Enhancing thermal conductivity of fluids with nanoparticles, ASME Fluids Engineering Division 231 (1995), 99-105.

[2] H. Adun, M. Abid, D. Kavaz, Y. Hu and J. H. Zaini, Optimizing the thermophysical behavior of a novel ternary hybrid nanofluid for energy applications through experimental research, Heliyon 10(12) (2024), e32728.

[3] J. Mohammed Zayan, A. K. Rasheed, A. John, W. F. Faris, A. Aabid, M. Baig and B. Alallam, Synthesis and characterization of novel ternary-hybrid nanoparticles as thermal additives, Materials 16(1) (2022), 173.

[4] N. S. Khashi'ie, M. F. Mukhtar, M. F. Abdollah, N. M. Arifin and I. Pop, Response surface-based optimization and sensitivity analysis of MHD tetra hybrid nanofluid flow over a shrinking disk, Chinese J. Phys. 96 (2025), 228-244.

[5] M. S. Elsherbiny, M. Ali, M. Shahin and M. El-Kady, Experimental study on the effect of micro concentrations of hybrid nanofluids through microchannel heat sinks, Journal of Applied and Computational Mechanics 11(2) (2025), 303-326.

[6] S. Yuan, Y. Leng, A. Fouly, E. M. Awwad, U. Nazir and M. Sohail, A study of four-phase fluid and thermal enhancement based on tetra-hybrid nanofluid considering temperature jump on a spinning sphere, Case Studies in Thermal Engineering 58 (2024), 104353.

[7] O. A. Oladapo, O. A. Ajala, A. O. Akindele, L. O. Aselebe, A. M. Obalalu, A. D. Ohaegbue and P. Adegbite, Analysis of variable properties on ternary and tetra hybrid nanofluids using Blasius Rayleigh-Stokes time dependent variable: a model for solar aeronautical engineering, International Journal of Thermofluids 23 (2024), 100775.

[8] Adnan, W. Abbas, M. Z. Bani-Fwaz and K. Kenneth Asogwa, Thermal efficiency of radiated tetra-hybrid nanofluid [(Al_2O_3-CuO-TiO_2-Ag)/water] tetra under permeability effects over vertically aligned cylinder subject to magnetic field and combined convection, Science Progress 106(1) (2023), 00368504221149797.

[9] F. N. Jamrus, I. Waini and A. Ishak, Time-depending flow of ternary hybrid nanofluid past a stretching sheet with suction and magnetohydrodynamic (MHD) effects, Journal of Advanced Research in Fluid Mechanics and Thermal Sciences 117(2) (2024), 15-27.

[10] F. N. Jamrus, A. Ishak, I. Waini and U. Khan, Radiative influence on axisymmetric ternary hybrid nanofluid flow with convective boundary conditions over a nonlinearly permeable stretching/shrinking disk, Internat. J. Numer. Methods Heat Fluid Flow 34(12) (2024), 4333-4361.

[11] F. N. Jamrus, A. Ishak, I. Waini, U. Khan, M. I. Siddiqui and J. K. Madhukesh, Aspects of non-unique solutions for Hiemenz flow filled with ternary hybrid nanofluid over a stretching/shrinking sheet, Advances in Mathematical Physics 2024(1) (2024), 7253630.

[12] F. N. Jamrus, A. Ishak, I. Waini, U. Khan, S. M. Hussain, J. K. Madhukesh and A. M. Abed, Stability scrutinization of a non-Newtonian (Williamson) ternary hybrid nanofluid past a stretching/shrinking sheet, ZAMM Z. Angew. Math. Mech. 105(2) (2025), e202300926.

[13] F. N. Jamrus, A. Ishak and I. Waini, Stability scrutinization of time depending flow of a ternary hybrid nanofluid past a shrinking sheet with wall mass suction effect, Malaysian Journal of Fundamental and Applied Sciences 20(3) (2024), 528-543.

[14] E. H. Aly and W. K. Usafzai, Multiple exact solutions of radiative micropolar hybrid nanofluid: Hiemenz flow, Journal of Nanofluids 13(4) (2024), 930-939.

[15] N. A. Zainal, N. S. Khashi'ie, I. Waini, A. R. Mohd Kasim, R. Nazar and I. Pop, Dual solutions for general three-dimensional MHD boundary layer stagnation-point flow of hybrid nanofluid and heat transfer, Internat. J. Numer. Methods Heat Fluid Flow 33(12) (2023), 4015-4036.

[16] I. Waini, A. Ishak and I. Pop, Hiemenz flow over a shrinking sheet in a hybrid nanofluid, Results in Physics 19 (2020), 103351.

[17] N. F. Ruslan, N. H. Norzawary, N. S. Wahid and M. E. Hafidzuddin, Heimenz flow over shrinking or stretching sheet in a ternary hybrid nanofluid, Semarak International Journal of Mechanical Precision Engineering 1(1) (2024), 44-55.

[18] M. Sarfraz and M. Khan, Heat transfer efficiency in planar and axisymmetric ternary hybrid nanofluid flows, Case Studies in Thermal Engineering 44 (2023), 102857.

[19] S. M. Sachhin, U. S. Mahabaleshwar, D. Zeidan, S. W. Joo and O. Manca, An effect of velocity slip and MHD on Hiemenz stagnation flow of ternary nanofluid with heat and mass transfer, Journal of Thermal Analysis and Calorimetry 150(4) (2025), 2533-2553.

[20] N. S. Khashi'ie, N. M. Arifin, M. Sheremet and I. Pop, Shape factor effect of radiative Cu-Al_2O_3/H_2O hybrid nanofluid flow towards an EMHD plate, Case Studies in Thermal Engineering 26 (2021), 101199.

[21] D. Khan, P. Kumam, W. Watthayu and F. Jarad, Exploring the potential of heat transfer and entropy generation of generalized dusty tetra hybrid nanofluid in a microchannel, Chinese J. Phys. 89 (2024), 1009-1023.

[22] I. Mahariq, H. A. Ghazwani and M. A. Shah, Enhancing heat and mass transfer in MHD tetra hybrid nanofluid on solar collector plate through fractal operator analysis, Results in Engineering 24 (2024), 103163.

[23] N. A. Zainal, R. Nazar, K. Naganthran and I. Pop, MHD flow and heat transfer of hybrid nanofluid over a permeable moving surface in the presence of thermal radiation, Internat. J. Numer. Methods Heat Fluid Flow 31(3) (2021), 858-879.

[24] N. A. Aladdin, N. Bachok and I. Pop, Cu-Al_2O_3/water hybrid nanofluid flow over a permeable moving surface in presence of hydromagnetic and suction effects, Alexandria Engineering Journal 59(2) (2020), 657-666.

[25] S. D. Harris, D. B. Ingham and I. Pop, Mixed convection boundary-layer flow near the stagnation point on a vertical surface in a porous medium: Brinkman model with slip, Transport in Porous Media 77(2) (2009), 267-285.